Available online at www.sciencedirect.com
SCIENCE DIRECT
Journal of Molecular Catalysis A: Chemical 252 (2006) 142–149
JOURNAL OF MOLECULAR CATALYSIS A: CHEMICAL
www.elsevier.com/locate/molcata

Comparative study of Au/Al_2O_3 and Au/CeO_2-Al_2O_3 catalysts

M.A. Centeno [a], K. Hadjiivanov [b,*], Tz. Venkov [b], Hr. Klimev [b], J.A. Odriozola [a]

[a] *Instituto de Ciencia de Materiales de Sevilla, Centro Mixto CSIC-Universidad de Sevilla, Avda Americo Vespuccio s/n, 41092 Sevilla, Spain*
[b] *Institute of General and Inorganic Chemistry, Bulgarian Academy of Sciences, Sofia 1113, Bulgaria*

Received 4 January 2006; received in revised form 20 February 2006; accepted 21 February 2006
Available online 29 March 2006

Abstract

Two gold-containing catalysts, Au/Al_2O_3 and Au/CeO_2-Al_2O_3, have been prepared by deposition–precipitation and characterized by different techniques (XRD, transmission electron microscopy (TEM), FTIR spectroscopy of adsorbed CO and catalytic test). The Au/CeO_2-Al_2O_3 sample demonstrates a much higher catalytic activity in the CO oxidation reaction than does the Au/Al_2O_3 sample. IR spectroscopy of adsorbed CO reveals that ceria generally keeps gold in a more oxidized state. Gold is in the form of Au^{3+} on the as-prepared samples. Low-temperature CO adsorption on the Au/Al_2O_3 sample evacuated at 473 K leads to the formation of Au^+–CO species evidencing reduction of Au^{3+} to Au^+. No gold carbonyls are detected on the Au/CeO_2-Al_2O_3 sample evacuated at the same temperature, this indicating that no auto-reduction has occurred. A carbonyl band at 2143 cm^{-1}, assigned to Au^+–CO species formed with Au^+ cations on metal gold particles, is registered after low-temperature CO adsorption on the Au/CeO_2-Al_2O_3 sample evacuated at 673 K, while CO adsorption on the Au/Al_2O_3 sample treated in the same way leads to the formation of Au^0–CO species (carbonyl band at 2106 cm^{-1}). Only metal gold was detected on the hydrogen-reduced Au/Al_2O_3 sample (carbonyl band at 2101 cm^{-1}) while on the Au/CeO_2-Al_2O_3 sample reduced with hydrogen, in addition to the metal gold (carbonyl band at 2108 cm^{-1}), Au^+ sites were also detected (carbonyl band at 2131 cm^{-1}). The role of the cationic gold sites in the CO oxidation reaction is discussed.

Keywords: Gold; Ceria; Infrared spectroscopy; Adsorption; Carbon monoxide; CO oxidation

1. Introduction

The interest in gold catalysts has continuously increased during the last years [1–49]. This interest has been provoked by the discovery that supported gold catalysts are very active in low-temperature CO oxidation when the gold is highly dispersed [1]. Since then, the researchers have been focusing efforts on three main areas: (i) understanding the origin of the catalytic activity of gold nanoclusters (nature of the active sites and reaction mechanism), (ii) optimization of the catalyst structure/composition and (iii) testing the gold catalysts in a series of other catalytic reactions. Despite the great number of studies, there are still many unresolved and debatable questions. For instance, it is not yet clear which is the oxidation state of the catalytically active gold. The hypothesis about the participation of the sites situated at the metal support interface, although gaining popularity, is not generally accepted either.

One of the most used techniques for characterization of supported catalysts is IR spectroscopy of probe molecules, especially CO [50–52]. It provides information on the oxidation and coordination state of surface-situated atoms/cations, their location, acidity, etc. There are many IR studies dealing with CO adsorption on supported gold [7–43]. However, the interpretation of the gold–carbonyl bands is also debatable. Based on the main principles of the use of CO as a probe molecule [50] and analysis of available literature data [7–43], we can infer the following: the most stable carbonyl complexes of gold are produced with participation of Au^+ cations. Note that a similar situation is encountered with copper and silver [50]. Indeed, bulk carbonyls of Au^+ are well known, but no bulk carbonyls of Au^0 have been described [53,54]. Consequently, CO adsorption on metallic gold results in formation of relatively unstable carbonyl species. According to Boccuzzi et al. [7,8], only particular Au^0 sites are active in CO adsorption and some gold planes are not able to adsorb CO even at low temperature.

Let us consider the other stable oxidation state of gold, namely Au^{3+}. In principle, coordinatively unsaturated Au^{3+} cations should absorb CO. However, these cations are usually

* Corresponding author. Tel.: +35 92 9793598; fax: +35 92 8705024.
E-mail address: kih@svr.igic.bas.bg (K. Hadjiivanov).

1381-1169/$ – see front matter © 2006 Elsevier B.V. All rights reserved.
doi:10.1016/j.molcata.2006.02.056

coordinatively saturated (blocked by water on the 'as prepared' samples). Activation, leading to removal of adsorbed water, in the case of gold catalysts results in auto-reduction of the Au^{3+} cations. That is why Au^{3+}–CO surface species are normally not detected.

In this work we report a comparative study of two gold-containing catalysts, Au/Al_2O_3 and Au/CeO_2-Al_2O_3, prepared by deposition–precipitation and sharply differing in their catalytic performance in the CO oxidation reaction. The Au/CeO_2-Al_2O_3 sample is much more active in both, oxidized and reduced states. To obtain information how the addition of cerium affects the state of gold, we have characterized the samples by different techniques (XRD, TEM, DR UV–vis) and mainly by FTIR spectroscopy of adsorbed CO. A disadvantage of the use of CO is that it can reduce the catalyst, thus modifying its properties. To avoid this, we have performed the experiments mainly at low temperatures (100 K). We have also studied co-adsorption of CO and O_2: according to data from the literature, this could minimize the reduction of the cationic gold [14,16,41].

2. Experimental

2.1. Preparation of the samples

The starting Al_2O_3 powder was aluminumoxid type C from Degussa (104 $m^2\,g^{-1}$). An impregnation method was used to prepare the CeO_2/Al_2O_3 support. The adequate amount of CeO_2 (Sigma, 99.9% pure) was dissolved in the smallest possible volume of 4 M HNO_3. Then, a slurry of Al_2O_3 powder in 200 ml of deionized water was added. The slurry thus prepared was taken into dryness by continuous stirring and heating (337–347 K). The solid was then kept overnight at 393 K in the oven, crushed in an agate mortar and calcined for 4 h at 873 K.

The gold-containing catalysts were prepared by deposition–precipitation. The adequate amount of $HAuCl_4{\cdot}3H_2O$ (Alfa, 99.99% pure) was dissolved in 150 ml of deionized water and the pH of the solution adjusted to 7.0 by addition of 0.1 M NaOH. The solution was heated to 343 K and then the support (as received Al_2O_3 or prepared CeO_2/Al_2O_3) was added and kept under continuous stirring for 1 h. The samples obtained were washed several times with deionized water (until the disappearance of Cl^- and Na^+ ions), then dried at 303 K. Fractions from the solids were finally calcined for 2 h at 773 K.

2.2. Characterization techniques

Chemical analysis of Au was performed by an ICP-AES Philips PV8250 spectrometer.

The specific surface area was determined according to the BET method by nitrogen adsorption measurements at liquid nitrogen temperature in a Micromeritics ASAP 2000 apparatus. Before analysis, the samples were degassed for 2 h at 423 K in vacuum.

XRD analysis was performed on a Siemens D 5000 powder X-ray diffractometer. Diffraction patterns were recorded with detector-sided Ni-filtered Cu Kα radiation (40 mA, 40 kV) over a 2θ-range of 22–74° and a position-sensitive detector using a step size of 0.010° and a step time of 2.5 s. The mean crystallite sizes were estimated using the Scherrer equation and the selected reflections peaks in the diffraction pattern were fitted by a Gaussian function. A peak broadening due to the instrumental broadening of $2\theta = 0.08°$ was taken into account.

Transmission electron microscopy (TEM) photographs were taken with a Philips CM200 microscope operating at 200 kV. The samples were dispersed in ethanol by sonication and dropped on a copper grid coated with a carbon film.

The IR spectra were recorded on a Nicolet Avatar 360 spectrometer at a spectral resolution of 2 cm^{-1} and accumulation of 64 scans. Self-supporting pellets (ca. 10 mg cm^{-2}) were prepared from the dried sample powder and treated directly in a purpose-made IR cell. The latter was connected to a vacuum-adsorption apparatus with a residual pressure below 10^{-3} Pa. Carbon monoxide (>99.997%) was supplied by Linde AG. Before use, it was additionally purified by passing through a liquid nitrogen trap. In order to minimize reactive CO adsorption and to be able to check for eventual $CO + O_2$ interaction, we studied adsorption of a $CO + O_2$ mixture in a molar ratio of 1:1. In what follows we shall refer to these experiments as CO adsorption experiments.

2.3. Catalytic measurements

Carbon monoxide oxidation was carried out in a conventional continuous flow U-shaped glass reactor (7 mm i.d.) under atmospheric pressure. An amount of 80 mg of the catalyst ($\phi < 100\,\mu m$) was placed between two plugs of glass wool. No activation procedure was performed over the fresh catalyst. Calcined Au/Al_2O_3 and $Au/CeO_2/Al_2O_3$ samples were activated for 2 h at 673 K under air (30 ml min^{-1}). The reactive mixture (84 ml min^{-1}) contained 2.5 mol% CO and 2.5 mol% O_2 in He. The gas analysis was performed by a Balzers Omnistar benchtop mass spectrometer.

3. Results

3.1. Initial characterization of the sample

Some characteristics of the samples are presented in Table 1. The gold content in the two samples was similar, which allowed comparison of their properties. It is also seen that gold deposition and calcination of the samples only slightly affect their

Table 1
Some characteristics of the samples investigated

Sample	Composition (wt%)			S_{BET} ($m^2\,g^{-1}$)
	Al	Au	Ce	
Al_2O_3	52.94	–	–	104.0
Au/Al_2O_3	48.00	1.91	–	Fresh: 101.7 Calcined: 93.9
CeO_2/Al_2O_3	39.45	–	14.95	87.9
$Au/CeO_2/Al_2O_3$	38.73	1.46	14.22	Fresh: 85.2 Calcined: 84.8

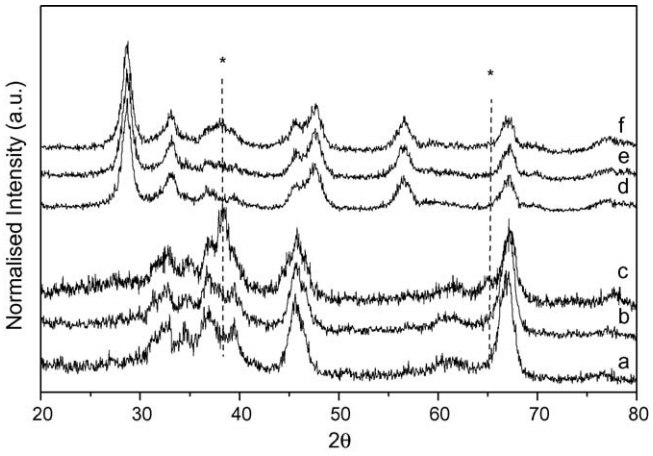

Fig. 1. XRD patterns of: Al_2O_3 (a); Au/Al_2O_3 fresh (b); Au/Al_2O_3 calcined (c); CeO_2/Al_2O_3 (d); $Au/CeO_2/Al_2O_3$ fresh (e); $Au/CeO_2/Al_2O_3$ calcined (f). Polycrystalline Au is labelled by '*'.

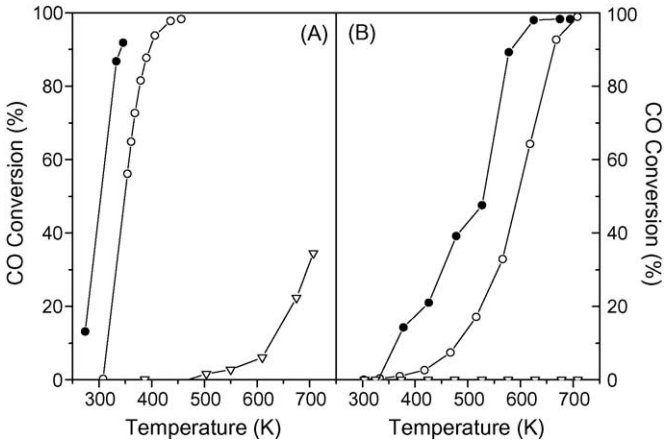

Fig. 2. Catalytic activity of the samples in the CO oxidation reaction. (A) CeO_2/Al_2O_3-based samples: (▽) CeO_2/Al_2O_3 support; (●) $Au/CeO_2/Al_2O_3$ fresh; (◯) $Au/CeO_2/Al_2O_3$ calcined. (B) Al_2O_3-based samples: (▽) Al_2O_3 support; (●) Au/Al_2O_3 fresh; (◯) Au/Al_2O_3 calcined.

specific surface areas. Only a small decrease of the surface area of the support was established after deposition of ceria on alumina.

The XRD of the fresh $Au/CeO_2/Al_2O_3$ sample showed no patterns due to gold, this indicating the absence of sufficiently large, if any, metal gold particles (Fig. 1, pattern b). However, metallic gold peaks were detected in the calcined sample (Fig. 1, pattern c). In this case the average size of the gold particles, as deduced from the broadening of the reflection gold peaks, was about 8.9 nm. These results agree with those obtained from the TEM observations. The mean gold particle size calculated from the particle size distribution in the TEM micrographs proves to be 8.2 nm for the calcined sample and below 2 nm for the fresh one. Note that TEM is not sensitive to the oxidation state of gold.

As in the case of Au/Al_2O_3, the XRD patterns of fresh $Au/CeO_2/Al_2O_3$ showed no peaks due to gold (Fig. 1, pattern e). Here again, the calcined sample showed a reflection characterizing metallic gold (Fig. 1, pattern f). Compared to the Au/Al_2O_3 sample, the gold peak was broader, suggesting a smaller average particle size. Indeed, the size of the gold crystallites, deduced from the broadening of the reflection gold peaks is, between 4.5 and 5.6 nm for the $Au/CeO_2/Al_2O_3$ sample and the CeO_2 crystalline size is about 8 nm. In addition, the intensity of the peak is lower, which suggests either a low crystallinity or incomplete reduction of gold.

The high atomic weight of cerium makes contrast differentiation of the gold particles on $Au/CeO_2/Al_2O_3$ samples difficult, although the more pronounced spherical shape of the gold particles helps. In the same way, particles with a very low diameter (typically, below 1 nm) are also difficult to detect due to the low mass and diffraction contrast. These factors probably drive to the main detection of the larger particles on the $Au/CeO_2/Al_2O_3$ catalysts. Taking in mind these events, the mean gold particle size, calculated from the particle size distribution in the TEM micrographs, results to be ca. 4.0 nm on the calcined $Au/CeO_2/Al_2O_3$ sample.

3.2. Catalytic activity

The results on the catalytic activities of the supports, the fresh and the calcined Au/Al_2O_3 and Au/CeO_2-Al_2O_3 samples are presented in Fig. 2. Alumina showed no activity in the CO oxidation reaction (Fig. 2B). Ceria on alumina demonstrated a low activity at high temperatures (Fig. 2A). This activity is related to the redox properties of ceria itself.

The fresh Au/Al_2O_3 sample showed an increasing activity in the range 330–620 K, the CO conversion reaching ca. 100%. The calcined sample was less active, with a kinetic curve shifted by ca. 70–100 K at higher temperatures (Fig. 2B).

A considerable activity was demonstrated by the fresh $Au/CeO_2/Al_2O_3$ sample even at 273 K (Fig. 2A). As in the case of Au/Al_2O_3, the calcined sample was less active. Here the kinetic curve was shifted by ca. 50 K at higher temperatures.

3.3. IR spectral characterization of the supports

In order to assign unambiguously the gold-containing species, it was necessary initially to characterize the supports. Here results will not be described in details for brevity. Generally, low-temperature CO adsorption on alumina activated at 673 K led to the appearance of a strong band at 2154 cm^{-1} (H-bonded CO) with a shoulder at 2185 cm^{-1} (Al^{3+}–CO). The Al^{3+}–CO band was more stable but also decreased in intensity and disappeared during evacuation at 100 K. At low coverages the bands were shifted to higher wavenumbers: the band at 2185 cm^{-1} was settled at 2194 cm^{-1} and the band at 2154 cm^{-1}, at 2160 cm^{-1}. The absence of bands above 2200 cm^{-1} is consistent with the relatively low activation temperature of the sample.

The spectra of the CeO_2/Al_2O_3 sample (as well as the spectra of gold supported on it) were characterized by a much higher level of the noise. In this case again H-bonded CO (2160 cm^{-1}) was detected after low-temperature CO adsorption. Two bands were detected at higher frequencies, at ca. 2190 and 2180 cm^{-1}. These are attributed to Al^{3+}–CO and Ce^{n+}–CO species, respectively [50,55,56].

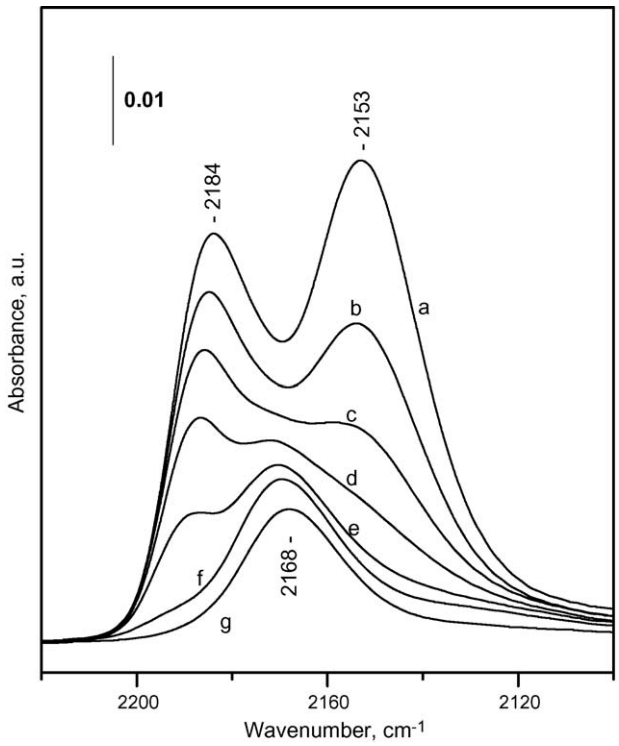

Fig. 3. FTIR spectra of $CO + O_2$ (1:1) co-adsorbed at 100 K on the Au/Al_2O_3 sample activated at 473 K. Initial CO equilibrium pressure of 665 Pa and evacuation at 100 K (a–f) and at ambient temperature (g).

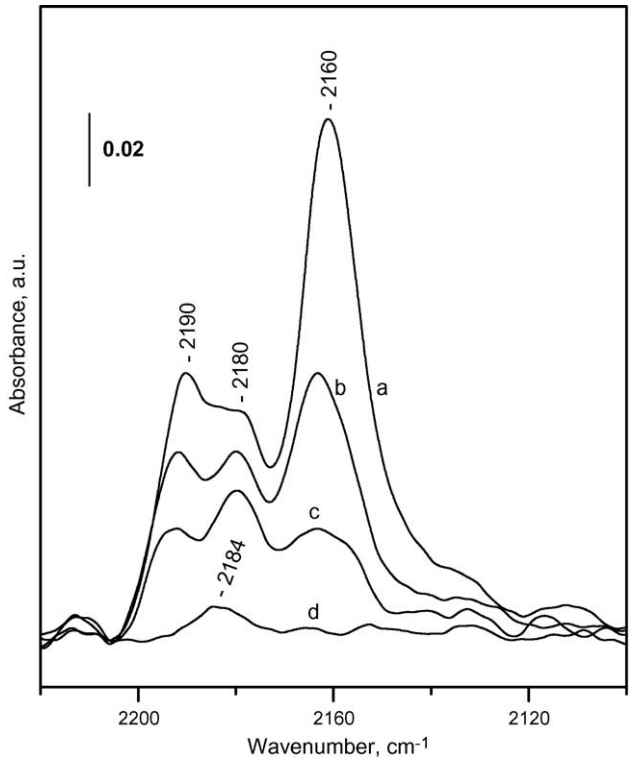

Fig. 4. FTIR spectra of $CO + O_2$ (1:1) co-adsorbed at 100 K on the $Au/CeO_2/Al_2O_3$ sample activated at 473 K. Initial CO equilibrium pressure of 665 Pa and evacuation at 100 K (a–c) and at increasing temperature (d).

3.4. CO adsorption on samples activated at 473 K.

Adsorption of a $CO + O_2$ mixture at 100 K on the Au/Al_2O_3 sample evacuated at 473 K results in the appearance of two bands, at 2184 and 2153 cm^{-1}, in the IR spectra (Fig. 3, spectrum a). They are assigned to Al^{3+}–CO and OH–CO species, respectively [50,55]. Evacuation leads to disappearance of these bands (the Al^{3+}–CO band shifted to 2191 cm^{-1}) and at low coverages a band at 2168 cm^{-1} is demasked (Fig. 3, spectra d–f). At ambient temperature only the band at 2168 cm^{-1} is recorded (Fig. 3, spectrum g). This band disappears from the spectrum after 373 K evacuation (not shown). Based on its stability and frequency, we assign the band at 2168 cm^{-1} to Au^+–CO species [11–19,21–23,39].

The same sets of experiments were performed with the $Au/CeO_2/Al_2O_3$ sample. In this case the low-temperature CO adsorption resulted in the appearance of three bands at 2190, 2180 and 2156 cm^{-1} (Fig. 4, spectrum a). All these bands were already observed with the support. A very weak feature at 2184 cm^{-1} remained after evacuation at ca. 300 K (Fig. 4, spectrum d). This band could characterize some carbonyls formed with the participation of cationic gold sites. Note, however, that this assignment is tentative.

3.5. CO adsorption on samples activated at 673 K

Low-temperature CO adsorption on the Au/Al_2O_3 sample evacuated at 673 K led to the appearance of the already described bands of Al^{3+}–CO (ca. 2195 cm^{-1}) and OH–CO (ca. 2160 cm^{-1}) (Fig. 5, spectrum a). Both bands are observed at higher frequencies as compared to the sample activated at 473 K. This is due to the additional sample dehydroxylation and creation of more acidic sites. In addition, a band at 2106 cm^{-1} is well seen.

The OH–CO band easily disappeared after evacuation even at low temperature (Fig. 5, spectra b and c). The Al^{3+}–CO band was more resistant but also declined (Fig. 5, spectra b–e). The band at 2106 cm^{-1} was the most stable one and was continuously blue shifted (to 2115 cm^{-1}) with the coverage decrease. However, this band also disappeared after evacuation at $T > 100$ K (Fig. 5, spectrum g). In agreement with literature data [7–17,19–25,27,29,32–37,41–43] we assign it to Au^0–CO species. Hence, the results demonstrate that increasing the evacuation temperature from 473 to 673 K leads to auto-reduction of the cationic gold sites on alumina and formation of metallic gold particles.

Low-temperature CO adsorption on the $Au/CeO_2/Al_2O_3$ sample that was preliminary evacuated at 673 K resulted in the appearance of bands at 2195, 2184, 2171 and 2143 cm^{-1} (Fig. 6, spectrum a). The bands at 2195 and 2184 cm^{-1} were already observed with the support and the sample activated at 473 K. Here they were somewhat blue shifted due to the higher activation temperature. The band at 2171 cm^{-1} disappeared very readily during evacuation (Fig. 6), i.e. it characterized a weak adsorption form and could not be due to Au^+–CO species. We assign this band to Ce^{3+}–CO carbonyls. Indeed, it has been reported that gold strongly accelerates the reducibility of ceria

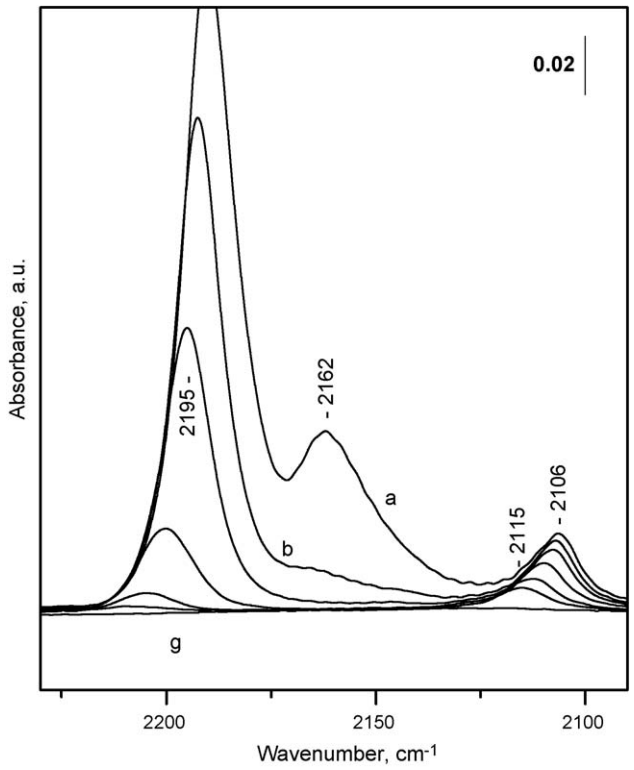

Fig. 5. FTIR spectra of $CO + O_2$ (1:1) co-adsorbed at 100 K on the Au/Al_2O_3 sample activated at 673 K. Initial CO equilibrium pressure of 665 Pa and evacuation at 100 K (a–f) and at ambient temperature (g).

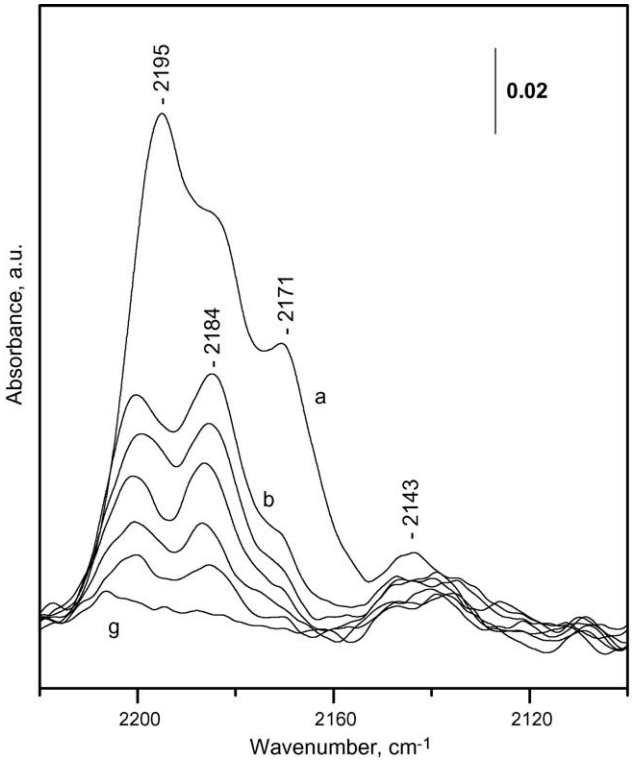

Fig. 6. FTIR spectra of $CO + O_2$ (1:1) co-adsorbed at 100 K on the $Au/CeO_2/Al_2O_3$ sample activated at 673 K. Initial CO equilibrium pressure of 665 Pa and evacuation at 100 K (a–d) and at increasing temperature (e–g).

[9,10]. The band at ca. 2143 cm^{-1} is the most resistant one towards evacuation. In a previous paper [16] we assigned a band in a similar position to Au^+–CO species, the gold cations being not dispersed on the support but located on the surface of the metal gold particles. In this way we explained the intermediate position and stability of the band: between the typical ones of Au^+–CO and Au^0–CO species. Taking into account the results with the hydrogen-reduced samples (see below) we support this earlier assignment. The observations can be rationalized assuming that the evacuation at 673 K has led to auto-reduction of gold. However, the surface of the metal particles (or at least the CO adsorption sites) has been reoxidized, the process being evidently promoted by the presence of ceria.

3.6. CO adsorption on reduced samples

Both gold-containing catalysts were reduced with hydrogen for 1 h at 473 K and then evacuated for 1 h at the same temperature. The spectra obtained after $CO + O_2$ co-adsorption on the reduced Au/Al_2O_3 sample (Fig. 7) were similar to those recorded with the calcined one. In this case, however, the Au^0–CO band was more intense (indicating a deeper auto-reduction of gold) and detected at somewhat lower frequencies (2101 cm^{-1}), which suggested increase of the main particle size.

The spectra of CO adsorbed at low temperature on the reduced $Au/CeO_2/Al_2O_3$ sample are presented in Fig. 8. In addition to the bands arising from CO adsorbed on the support, in this case we detected Au^0–CO species by a band at 2108 cm^{-1}. The band position suggested a higher dispersion of gold, as compared to

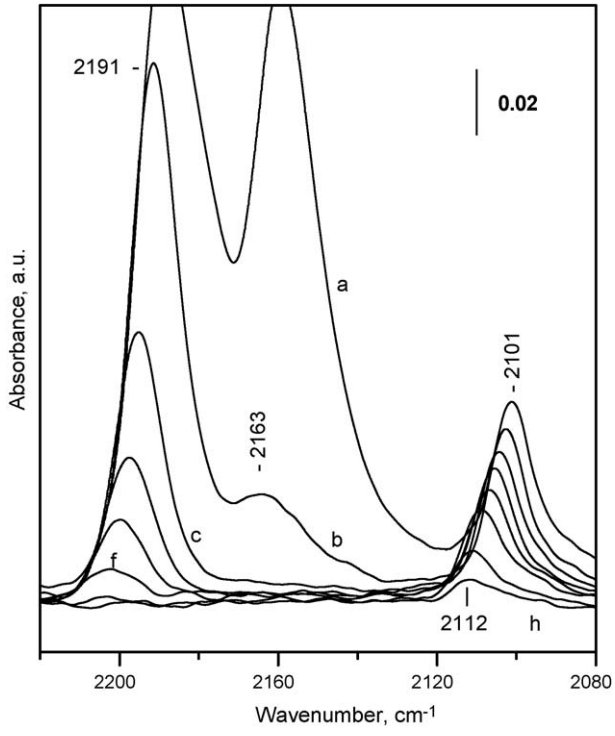

Fig. 7. FTIR spectra of $CO + O_2$ (1:1) co-adsorbed at 100 K on H_2-reduced Au/Al_2O_3 sample. Initial CO equilibrium pressure of 665 Pa and evacuation at 100 K (a–g) and at increasing temperature (h).

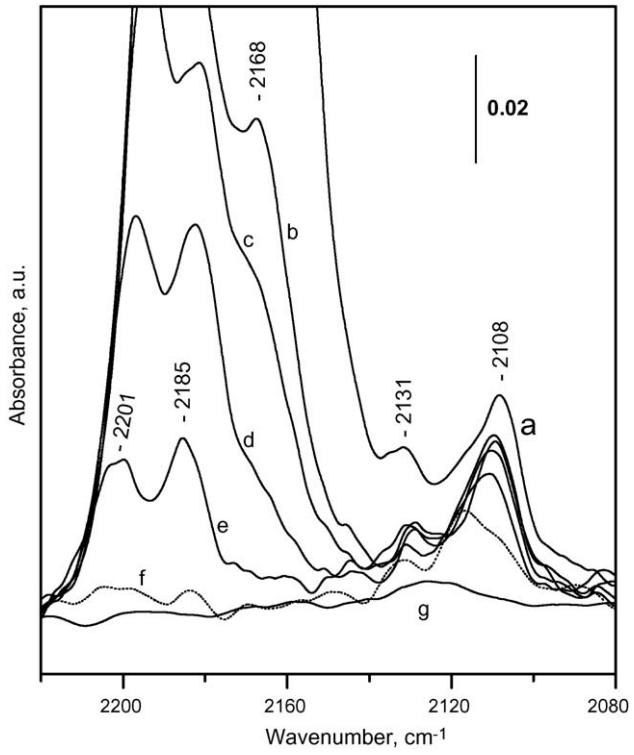

Fig. 8. FTIR spectra of $CO + O_2$ (1:1) co-adsorbed at 100 K on H_2-reduced $Au/CeO_2/Al_2O_3$ sample. Initial CO equilibrium pressure of 665 Pa and evacuation at 100 K (a–d) and at increasing temperatures (e–g).

the Au/Al_2O_3 sample, which is consistent with the XRD observations. A careful analysis of the spectra shows also the existence of a weak band around 2131 cm^{-1} which characterizes relatively stable species. Bands in similar positions have already been assigned to CO adsorbed on Au^+ cations situated on metallic gold particles. Thus, it appears that even after reduction with hydrogen, some cationic gold sites are present on the catalyst surfaces under the experimental condition used. Evidently, this stabilisation of cationic gold is due to the presence of ceria. Indeed, a broad band around 2120 cm^{-1} is well seen after sample evacuation (Fig. 8, spectrum g) and is probably present in the preceding spectra. This band is likely due to an electronic transition, typical of reduced ceria [56–58]. The appearance of this band suggests that ceria oxidizes gold sites.

4. Discussion

In order to draw conclusions on the state of gold on the different catalysts after various pretreatments, it is necessary to assign unambiguously the IR carbonyl bands. For convenience, the assignments are summarised in Table 2.

Let us first consider the possibility of detection of Au^{3+}–CO bands. Since gold was initially deposited on both catalysts as Au^{3+} species, some of them may be present on the samples activated at 473 K. It is known that interaction of CO with highly charged cations is essentially electrostatic and the stretching frequency of adsorbed CO depends on the electrostatic field of the cation [50,51]. Ca^{2+} cations (radius of 0.99 Å) in CaNaY form Ca^{2+}–CO species absorbing at 2200 cm^{-1} [59]. Taking into account the higher charge of Au^{3+} and the lower ionic radius (0.85 Å [60]), the frequency at which the Au^{3+}–CO carbonyls in zeolites are expected is higher than 2200 cm^{-1}. Indeed, some of us [30] have detected Au^{3+}–CO species at 2207 cm^{-1} in a Au/NaY sample prepared using a $Au^{3+}(CH_3)_2(C_5H_7O_2)$ precursor. In this case contact of the sample with air was prevented in all experiments, starting from the preparation and passing through the pellet preparation and transfer into the IR cell. Evacuation led to removal of the organic ligands and some Au^{3+} ions migrated to cationic positions. However, this frequency could be lower when Au^{3+} ions are not in cationic position or supported on oxides. For comparison: Cu^+–CO species formed with Cu^+ cations exchanged in ZSM-5 zeolite absorb at 2158 cm^{-1} [61,62], while the same species formed with Cu^+ ions on oxides or in zeolites, but not in cationic positions, are observed at ca. 2130 cm^{-1} [62,63]. Hence, one can expect that Au^{3+}–CO carbonyls should be detected at frequencies down to ca. 2180 cm^{-1}. Note that these species should be unstable because of the nature of the Au^{3+}–CO bond, namely due to electrostatic interaction.

Analysis of the spectra presented in Figs. 3 and 4 does not provide evidence of Au^{3+}–CO species. Most probably, if Au^{3+} ions exist, they should be coordinatively saturated and not detectable by CO even at low temperature. However, the existence of some amount of Au^{3+}–CO species cannot be totally ruled out, the respective bands having been masked by the strong carbonyl bands of the support observed in the region. The weak band at 2184 cm^{-1} (Fig. 4, spectrum d) could characterize carbonyls of Au^{3+} ions.

As already said in Section 1, the most stable gold carbonyls are those of the Au^+ cations. This is due to the bonding of CO to Au^+ sites by σ- and π-back bonds and the strong synergism between them. Increase of the effective charge of the Au^+ sites reflects in a strengthening of the σ-bond between Au^+ and CO and increase of the CO stretching frequency. As a result of the synergistic effect, the π-bond will also be strengthened. This, on its part, should lead to some decrease of the CO stretching frequency and increase of the overall Au^+–CO bond strength.

Table 2
Assignment of the gold–carbonyl bands

Species	Bands (cm^{-1})	Comment
Au^+–CO formed on isolated Au^+ ions	2168	Registered with Au/Al_2O_3 sample evacuated at 473 K
Au^+–CO formed on Au^+ ions from the surface of metal particles	2143	Registered with $Au/CeO_2/Al_2O_3$ sample evacuated at 673 K
	2130	Registered with the reduced $Au/CeO_2/Al_2O_3$ sample
Au^0–CO formed on particular Au^0 atoms only	2115–2101	Registered with the reduced samples and the Au/Al_2O_3 sample evacuated at 673 K

However, the increase of the effective charge of the cation alone should reflect in the decrease of the π-bond order. A detailed analysis of these effects has been provided for the Cu^+–CO [62] and Ag^+–CO systems [64]. It has been concluded that the π-bond for the Cu^+–CO system is only slightly enhanced with the increase of the effective charge of the cation [62]. With Au^+, where the π-back donation is less important than for the Cu^+ cations, the change of the π-bond order should be even weaker. Hence, the stability and the frequency of the Au^+–CO species can well be interpreted using the conception of the σ-bond alone.

With the Au/Al_2O_3 sample calcined at 473 K we detected a stable towards evacuation band at 2168 cm^{-1} (Fig. 3) which is therefore unambiguously assigned to Au^+–CO species. Under these conditions no metallic gold was produced, so we can conclude that the band characterizes isolated gold sites. Similar bands have been described by many researches [11–19,21–23,39] and with minor exceptions assigned to Au^+–CO species. Pestryakov et al. [11] detected a band at 2175 cm^{-1} with a Au/Al_2O_3 sample. The somewhat higher position of the band, as compared to the observation reported here, is most probably due to the presence of a large amount of chlorine ions (enhancing the Au^+ electrophilicity) in their sample. Comparison with the literature data [17–23,39] shows that Au^+–CO species in zeolites are observed at somewhat higher frequencies, which is consistent with the already discussed higher electrophilicity of cations exchanged in zeolites.

The next species to be considered are the Au^0–CO carbonyls. Many observations point out that only a fraction of the metallic gold sites are able to adsorb CO even at low temperature. Note that metal silver is also inert to CO and only particular sites can form carbonyls [65]. According to Boccuzzi et al. [7,8], CO is adsorbed on step sites on the metal particles. So, we can divide the metallic gold surface sites into two general groups: (i) inert sites (Au^0_{in}) and active sites (Au^0_{act}). The results of this study confirm that the higher the dispersion of the supported metal gold, the higher the CO stretching frequency of the Au^0_{act}–CO species.

Many authors assign bands in the 2155–2130 cm^{-1} region to carbonyls formed with the participation of positively charged gold species [7,10,11,15,16,20,27,29,31] or gold atoms with adsorbed oxygen [12,13,24]. In a previous study of the Au/Al_2O_3 sample [16], we observed a band at 2140 cm^{-1} appearing after CO adsorption on a sample treated under oxygen at 673 K and then evacuated at 473 K. Since XRD showed metallic particles on the calcined samples, we assigned this band to Au^+–CO species, the Au^+ cations being situated on the metal particles. In this way these cations are able to transmit positive charge to the gold bulk, which explains the lower frequency and lower stability of the respective carbonyls as compared to the carbonyls of isolated Au^+ sites. Since no Au^0–CO species were simultaneously detected, we can conclude that the (Au^0_{act}) sites on Au/Al_2O_3 are easily oxidized at 673 K.

A similar band (at 2143 cm^{-1}) was observed in this study with the $Au/CeO_2/Al_2O_3$ sample calcined at 673 K (Fig. 6). Therefore, we can stress that with this sample, calcination has led to reduction of the gold to metal and subsequent reoxidation of the Au^0_{act} sites to Au^+ cations. Evidently, ceria promotes this oxidation, since no such band was detected with the Au/Al_2O_3 sample subjected to an analogous treatment. This model also explains the relatively low intensity of the 2143 cm^{-1} band.

A weak carbonyl band at 2131 cm^{-1} was detected on the reduced $Au/CeO_2/Al_2O_3$ sample. We assign this band again to Au^+–CO species formed with Au^+ cations on the surface of the metal gold particles. The lower frequency of this band (as compared to the band observed with the 473 K calcined sample) is most probably due to the increase of the metal gold particle size, allowing a more effective charge transfer from Au^+ to the gold bulk. As a result, the electrophilicity of the Au^+ sites decreases and the frequency of adsorbed CO is red shifted. The results evidence that ceria promotes the oxidation of the Au^0_{act} sites. As already discussed, this interpretation is supported by the appearance of a band around 2120 cm^{-1} typical of reduced ceria. We can speculate that after reduction of the sample, a strong metal–support interaction (SMSI) effect takes place. SMSI is characterized by partial covering the metal particle with suboxide phase from the support [66]. Thus, ceria can affect more gold sites.

All results of this study show that addition of ceria stabilises a more oxidized state and a higher dispersion of gold. With the Au/Al_2O_3 sample we observed that calcination at 473 K led to formation of Au^+ species. However, no gold carbonyls were evidenced with the $Au/CeO_2/Al_2O_3$ sample evacuated at 473 K. This observation can be rationalized assuming that gold on this sample is encountered as Au^{3+} species which are coordinatively saturated. Evacuation of a Au/Al_2O_3 pellet at 673 K led to full auto-reduction of gold (see Fig. 4), while only Au^+ cations situated on the metal particles were detected with the $Au/CeO_2/Al_2O_3$ sample calcined at the same temperature (see Fig. 5). Even on the reduced $Au/CeO_2/Al_2O_3$ sample some fraction of Au^+ sites existed. This means that addition of ceria inhibits the reduction of cationic gold and/or promotes the oxidation of the Au^0_{act} sites.

These observations coupled with the high catalytic activity of the sample in CO oxidation strongly support the idea about the decisive role of the Au^+ cations in the reaction. Comparison between the kinetic curves of the calcined samples suggests that oxidized Au^0_{act} sites (or the respective redox couples) play a role in the reaction mechanism. However, the higher activity of the fresh sample indicates that isolated cationic gold species are even more active that the Au^+ species from the surface of the gold particles, as already suggested [28].

5. Conclusions

Addition of ceria to an alumina support strongly enhances the catalytic activity of supported gold in the CO oxidation reaction. This effect is due to: (i) the higher dispersion of gold on CeO_2/Al_2O_3 as compared to Al_2O_3 and (ii) a strong promoting effect of ceria in the oxidation of the Au^0 sites for CO adsorption. Evidence was also found that isolated Au^+ sites are more active in CO oxidation than metallic gold particles.

Acknowledgments

The financial support by the projects CSIC/BAS (2004BG0001) and FP6-2004-ACC-SSA-2 is gratefully acknowledged.

References

[1] M. Haruta, T. Kobayashi, H. Sano, N. Yamada, Chem. Lett. (1987) 405.
[2] R. Meyer, C. Lemire, Sh.K. Shaikhutdinov, H.-J. Freund, Gold Bull. 37 (2004) 72.
[3] G.C. Bond, D.T. Thompson, Catal. Rev. Sci. Eng. 41 (1999) 319.
[4] M. Haruta, Gold Bull. 37 (2004) 27.
[5] M.I. Dominguez, M. Sánchez, M.A. Centeno, M. Montes, J.A. Odriozola, Appl. Catal. A 302 (2006) 96.
[6] M.A. Centeno, M. Paulis, M. Montes, J.A. Odriozola, Appl. Catal. B 61 (2005) 77.
[7] F. Boccuzzi, A. Chorino, S. Tsubota, M. Haruta, J. Phys. Chem. 100 (1996) 3625.
[8] F. Boccuzzi, A. Chorino, Stud. Surf. Sci. Catal. 140 (2001) 77.
[9] T. Tabakova, F. Boccuzzi, M. Manzoli, D. Andreeva, Appl. Catal. A 252 (2003) 385.
[10] T. Tabakova, F. Boccuzzi, M. Manzoli, J.W. Sobczak, V. Idakiev, D. Andreeva, Appl. Catal. B 49 (2004) 73.
[11] A. Pestryakov, V. Lunin, A. Kharlanov, D. Kochubey, N. Bogdanchikova, A. Stakheev, J. Mol. Struct. 642 (2002) 129.
[12] S. Minico, S. Scire, C. Crisafalli, A.M. Visco, S. Galvagno, Catal. Lett. 47 (1997) 273.
[13] D.J.C. Yates, J. Colloid Interface Sci. 29 (1969) 194.
[14] M.A.P. Dekkers, M.J. Lippits, B.E. Nieuwenhuys, Catal. Lett. 56 (1998) 195.
[15] Tz. Venkov, K. Fajerwerg, L. Delannoy, Hr. Klimev, K. Hadjiivanov, C. Louis, Appl. Catal. A 301 (2006) 106.
[16] Tz. Venkov, Hr. Klimev, M.A. Centeno, J.A. Odriozola, K. Hadjiivanov, Catal. Commun. 7 (2006) 308.
[17] T.M. Salama, R. Ohnishi, T. Shido, M. Ichikawa, J. Catal. 162 (1996) 169.
[18] S. Qiu, R. Ohnishi, M. Ichikawa, J. Phys. Chem. 98 (1994) 2719.
[19] K. Okumura, K. Yoshino, K. Kato, M. Niwa, J. Phys. Chem. B 109 (2005) 12380.
[20] G. Riahi, D. Guillemont, M. Polisset-Thfoin, A. Khodadadi, J. Fraissard, Catal. Today 72 (2002) 115.
[21] M. Mohamed, T. Salama, R. Onishi, M. Ichikawa, Langmuir 17 (2001) 5678.
[22] M. Mohamed, T. Salama, M. Ichikawa, J. Colloid Interface Sci. 224 (2000) 366.
[23] D. Akolekar, S.K. Bhargava, J. Mol. Catal. A 236 (2005) 77.
[24] F. Boccuzzi, A. Chiorino, J. Phys. Chem. B 104 (2000) 5414.
[25] S. Carrettin, A. Corma, M. Iglesias, F. Sanchez, Appl. Catal. A 291 (2005) 247.
[26] D. Boyd, S. Golunski, G. Hearne, T. Magadzu, K. Mallick, M. Raphulu, A. Venygopal, M. Scurrell, Appl. Catal. A 292 (2005) 76.
[27] J.-D. Grunwaldt, M. Maciejewski, O. Becker, P. Fabrizioli, A. Baiker, J. Catal. 186 (1999) 458.
[28] C. Fierro-Gonzalez, B.C. Gates, J. Phys. Chem. B 108 (2004) 16999.
[29] D. Guillemot, V. Borokov, V. Kazansky, M. Polisset-Thfoin, J. Fraissard, J. Chem. Soc. Faraday Trans. 93 (1997) 3587.
[30] M. Mihaylov, J.C. Fierro-Gonzalez, H. Knözinger, B.C. Gates, K. Hadjiivanov, J. Phys. Chem. B, in press.
[31] J.C. Fierro-Gonzalez, B.G. Anderson, K. Ramesh, C.P. Vinod, J.W.H. Niemantsverdried, B.C. Gates, Catal. Lett. 101 (2005) 265.
[32] M.A. Bollinger, M.A. Vannice, Appl. Catal. B 8 (1996) 417.
[33] H. Liu, A.I. Kozlov, A.P. Kozlova, T. Shido, K. Asakura, Y. Iwasawa, J. Catal. 185 (1999) 252.
[34] K. Mallick, M.J. Witcomb, M.S. Scurrell, Appl. Catal. A 259 (2004) 163.
[35] B. Schumacher, V. Plzak, M. Kinne, R.J. Behm, Catal. Lett. 89 (2003) 109.
[36] S. Overburya, L. Ortiz-Soto, H. Zhu, B. Leeb, M.D. Amiridis, S. Dai, Catal. Lett. 95 (2004) 99.
[37] J.L. Margitfalvi, A. Fasi, M. Hegedus, F. Lonyi, S. Gobölös, N. Bogdanchikova, Catal. Today 72 (2002) 157.
[38] M. Debeila, N.J. Coville, M.S. Scurrell, G.R. Hearne, Appl. Catal. A 291 (2005) 98.
[39] Z.-X. Gao, Q. Sun, H.Y. Chen, Z. Wang, W.M.H. Sachtler, Catal. Lett. 72 (2001) 1.
[40] J. Yang, J. Henao, M. Raphulu, Y. Wang, T. Kaputo, A. Groszek, M.C. Kung, M. Scurrell, J. Miller, H.H. Kung, J. Phys. Chem. B 109 (2005) 10319.
[41] A. Tripathi, V. Kamble, N. Gupta, J. Catal. 187 (1999) 332.
[42] J. Jia, J.N. Kondo, K. Domen, K. Tamara, J. Phys. Chem. B 105 (2001) 3017.
[43] Y. Jugnet, F.J. Cadete Santos Aires, C. Deranlot, L. Piccolo, J.C. Bertolini, Surf. Sci. 521 (2002) L639.
[44] M.A. Centeno, C. Portales, I. Carrizosa, J.A. Odriozola, Catal. Lett. 102 (2005) 289.
[45] M.A. Centeno, M. Paulis, M. Montes, J.A. Odriozola, Appl. Catal. A 234 (2002) 65.
[46] M.A. Centeno, I. Carrizosa, J.A. Odriozola, Appl. Catal. A 246 (2003) 365.
[47] I.N. Remediakis, N. Lopez, J.K. Nørskov, Appl. Catal. A 291 (2005) 13.
[48] T.V. Choudhary, D.W. Goodman, Appl. Catal. A 291 (2005) 32.
[49] P.X. Huang, F. Wu, B.L. Zhu, X.P. Gao, H.Y. Zhu, T.Y. Yan, W.P. Huang, S.H. Wu, D.Y. Song, J. Phys. Chem. B 109 (2005) 19169.
[50] K. Hadjiivanov, G. Vayssilov, Adv. Catal. 47 (2002) 347.
[51] H. Knözinger, in: G. Ertl, H. Knözinger, J. Weitkamp (Eds.), Handbook of Heterogeneous Catalysis, vol. 2, Wiley/VCH, Weinheim, 1997.
[52] A. Davydov, Molecular Spectroscopy of Oxide Catalyst Surfaces, Wiley, Chichester, 2003.
[53] F. Aubke, C. Wang, Coord. Chem. Rev. 137 (1994) 483.
[54] Q. Xu, Coord. Chem. Rev. 231 (2001) 83.
[55] H. Knözinger, P. Ratnasamy, Catal. Rev. Sci. Eng. 17 (1978) 31.
[56] C. Binet, M. Daturi, J.C. Lavalley, Catal. Today 50 (1999) 207.
[57] A. Diaz, S. Guillope, P. Verdier, Y. Laurent, A. Lopez, J. Sambeth, A. Paul, J.A. Odriozola, Mater. Sci. Forum 325 (2000) 283.
[58] M.A. Centeno, I. Carrizosa, J.A. Odriozola, Appl. Catal. B 19 (1998) 67.
[59] K. Hadjiivanov, H. Knözinger, J. Phys. Chem. B 105 (2001) 4531.
[60] R.D. Shannon, Acta Cryst. A 32 (1976) 751.
[61] G. Spoto, A. Zecchina, S. Bordiga, G. Ricchiardi, C. Martra, G. Leofanti, G. Petrini, Appl. Catal. B 3 (1994) 151.
[62] K. Hadjiivanov, M. Kantcheva, D. Klissurski, J. Chem. Soc. Faraday Trans. 92 (1996) 4595.
[63] K. Hadjiivanov, D. Klissurski, G. Ramis, G. Busca, Appl. Catal. B 7 (1996) 251.
[64] K. Hadjiivanov, H. Knözinger, J. Phys. Chem. B 102 (1998) 10936.
[65] J. Müslehiddinoglu, M.A. Vannice, J. Catal. 213 (2003) 305.
[66] K. Hadjiivanov, D. Klissurski, Chem. Soc. Rev. 25 (1996) 61.